Localization of the Unruh Effect

Kevin Player*

June 15, 2025

> The Unruh effect tells us that what we call particles is really just a matter of perspective.
>
> Lee Smolin

Abstract

We present a framework that interpolates between the conventional thermal description of the Unruh effect and a fully localized, non-thermal excitation. In a uniformly accelerating frame, the extended support of Rindler modes across the wedge leads to red- and blue-shifted components, mixing frequencies in a manner that gives rise to the familiar thermal response. To refine this picture, we introduce a partially localized perspective: using modular automorphisms, we map modes between nested Rindler wedges and analyze their localization properties. We further interpolate to compactly supported wave modes using parabolic cylinder functions, enabling a smooth transition from global to local behavior. While the standard interpretation attributes particle detection to horizon thermality, our construction suggests an alternative mechanism, modeling the observed response as arising from thrust: a localized, directed energy input into the field. This provides a mechanistic account that complements the statistical explanation typically associated with the effect.

1 Introduction

The Unruh effect[1] reveals that uniformly accelerated observers perceive the Minkowski vacuum as a thermal state, detecting a bath of particles where inertial observers see none. This phenomenon is often presented by comparing positive-frequency Minkowski modes to Rindler modes, leading to Bogoliubov transformations that mix creation and annihilation operators[2]. The standard explanation relies on the global nature of Rindler modes, which span the entire wedge and undergo both red-shift and blue-shift along their support.

In this work, we develop a complementary viewpoint by examining how localization affects the thermal character of the response. In Section 2, we review of the Unruh effect, including the relevant mode expansions and Bogoliubov transformations. In Section 3, we apply a classical source construction [3] to inject particles into the field. When targeted at negative-frequency Unruh modes, this setup reproduces the familiar Rindler particle spectrum predicted by the Bogoliubov analysis.

Section 4 explores partial localization by considering sub-regions of the Rindler wedge related through space-like translations and reflections, transformations that correspond

*kjplaye@gmail.com

to modular automorphisms in the associated operator algebras. We then use parabolic cylinder functions to construct smooth interpolations between eternal Rindler modes and fully localized modes. Finally, in Section 5, we interpret the implications of this construction. These results suggest an alternative interpretation: that the Unruh effect may be understood in terms of localized, non-thermal field excitations that resemble a thrust-like driving force on the field.

2 Preliminaries

We draw notation and standard results from Frodden and Valdés [4] and T. Jacobson [5].

Let $\hbar = c = 1$. We consider a uniformly accelerating observer in 1+1 dimensional Minkowski spacetime with metric signature $\eta = (-1, +1)$. The extension to 1+3 dimensions does not affect the key physics of the Unruh effect, so we restrict to the (t,x) plane where the boost is occurring.

Consider the free scalar massless Lagrangian

$$\mathcal{L}_{free} = -\frac{1}{2}\eta^{\mu\nu}\partial_\mu\phi\partial_\nu\phi. \tag{1}$$

We consider positive frequency modes with dispersion relation $\omega_k = |k| > 0$ as solutions to the resulting Klein-Gordon equation

$$\Box\phi = -\frac{\partial^2\phi}{\partial t^2} + \frac{\partial^2\phi}{\partial x^2} = 0, \tag{2}$$

where $\Box = \eta^{\mu\nu}\partial_\mu\partial_\nu$. We expand ϕ in terms of ladder operators $a_k, a_k^\dagger$

$$\phi(x,t) = \int \mathrm{d}k\, a_k\varphi_k(x,t) + \text{h.c.} \tag{3}$$

where

$$\varphi(x,t) = \frac{1}{\sqrt{4\pi\omega_k}}e^{i(kx-\omega_k t)}. \tag{4}$$

are pure Minkowkski positive frequency waves normalized with respect to the Klein-Gordon inner product over a Cauchy surface Σ (usually $t = 0$)

$$\langle f, g\rangle_{KG} = i\int_\Sigma \mathrm{d}x(f^*\partial_t g - \partial_t f^* g). \tag{5}$$

2.1 Rindler Coordinates

To describe the physics from the point of view of a uniformly accelerating observer, we introduce Rindler coordinates [4, 6] covering a right wedge

$$W = \{(x,t) : x > |t|\} \tag{6}$$

with apex at the origin, corresponding to region I pictured[1] in Figure 1; with coordinates

$$t = \frac{1}{a}e^{a\xi}\sinh(a\eta) \tag{7}$$

$$x = \frac{1}{a}e^{a\xi}\cosh(a\eta) \tag{8}$$

The constant acceleration parameter a is introduced explicitly to make the dependence of the Unruh temperature, $T = \frac{a}{2\pi}$, manifest in subsequent expressions. The coordinates (η, ξ) describe the proper time and position in the frame of a uniformly accelerating observer,

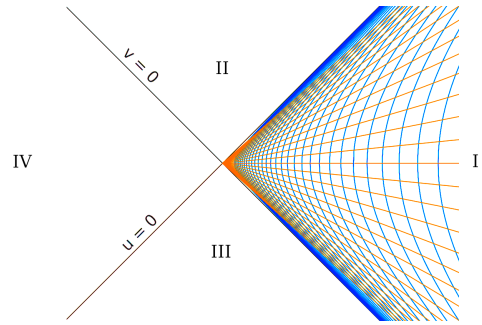

Figure 1: Rindler wedge I on the right.

with world-lines of constant ξ corresponding to hyperbolic trajectories in Minkowski space-time.

The massless Klein-Gordon equation in Rindler coordinates is

$$\Box\phi = e^{-2a\xi}(-\partial_\eta^2 + \partial_\xi^2)\phi = 0 \tag{9}$$

The wave equation retains the same structure as the Minkowski case, up to the overall conformal factor $e^{-2a\xi}$. Since this factor does not affect the null structure of the equation, the mode solutions retain the same plane wave form but in the Rindler coordinates

$$r_k(\eta, \xi) = \frac{1}{\sqrt{4\pi\omega_k}} e^{-i(\omega_k\eta - k\xi)} + \text{h.c.} \tag{10}$$

for each wave number k and positive frequency $\omega_k = |k| > 0$. These "Rindler modes" are in terms of η and ξ and are thus confined to the Rindler wedge W. Since Rindler coordinates only cover region I (the right wedge), these modes are not defined globally in Minkowski space.

2.2 Unruh Modes

To understand how a uniformly accelerated observer perceives the Minkowski vacuum as a thermal bath, we construct the Unruh modes, analytic combinations of Rindler modes that correspond to positive-frequency solutions with respect to Minkowski time.

From now on let $\omega_k = k > 0$. Bogoliubov coefficients satisfy $\alpha_k^2 - \beta_k^2 = 1$, ensuring normalization. The expressions below reflect their standard form and the associated thermal weighting:

$$\begin{aligned} \alpha_k &= \frac{e^{\frac{\pi\omega_k}{2a}}}{\sqrt{2\sinh\frac{\pi\omega_k}{a}}} = \sqrt{\frac{1}{1 - e^{-2\pi\omega_k/a}}} \\ \beta_k &= \frac{e^{\frac{-\pi\omega_k}{2a}}}{\sqrt{2\sinh\frac{\pi\omega_k}{a}}} = \sqrt{\frac{1}{e^{2\pi\omega_k/a} - 1}} \quad \text{(thermal form)} \end{aligned} \tag{11}$$

We analytically continue[2] the Rindler modes r_k and r_{-k} into the (t, x) plane, with $i\epsilon$ prescription, to understand their frequency content with respect to Minkowski time. This continuation reveals a change in frequency character (positive to negative) across the branch cut[3]

$$\begin{aligned} r_{+k} &= \frac{1}{\sqrt{4\pi\omega_k}} e^{-i(\omega_k\eta - k\xi)} = \frac{1}{\sqrt{4\pi\omega_k}} (a(-t + x + i\epsilon))^{\frac{i\omega_k}{a}} \\ r_{-k} &= \frac{1}{\sqrt{4\pi\omega_k}} e^{-i(\omega_k\eta + k\xi)} = \frac{1}{\sqrt{4\pi\omega_k}} (a(t + x - i\epsilon))^{\frac{-i\omega_k}{a}} \end{aligned} \tag{12}$$

[1] All diagrams follow the convention of t increasing upward and x increasing to the right.

[2] From the definitions and properties of sinh and cosh, it follows that $a(\mp t + x) = e^{a(\pm\eta + \xi)}$.

[3] Specifically $r_{\pm k} = e^{\pm\frac{i\omega_k}{a}\log a(\mp t + x \pm i\epsilon)}$.

Although r_k and r_{-k} are positive-frequency modes with respect to Rindler time η, analytic continuation across the branch cut into the left wedge reveals that they acquire negative-frequency components with respect to Minkowski time t; see the middle column in Figure 2.

We recall the standard Minkowski positive-frequency plane wave modes, here with $k > 0$:

$$\begin{aligned} \varphi_{+k} &= \frac{1}{\sqrt{4\pi\omega_k}} e^{-i(\omega_k t - kx)} \\ \varphi_{-k} &= \frac{1}{\sqrt{4\pi\omega_k}} e^{-i(\omega_k t + kx)} \end{aligned} \tag{13}$$

We next construct the Unruh modes

$$\begin{aligned} \mu_k^R &= \alpha_k r_{+k} + \beta_k \widetilde{r^*_{-k}} = \alpha_k r_{+k} - \beta_k l_{-k} \\ &= \frac{1}{\sqrt{4\pi\omega_k}\sqrt{2\sinh\frac{\pi\omega_k}{a}}} \left(e^{\frac{\pi\omega_k}{2a}} \left(a(-t+x+i\epsilon)\right)^{\frac{i\omega_k}{a}} + e^{\frac{-\pi\omega_k}{2a}} \left(a(t+x-i\epsilon)\right)^{\frac{i\omega_k}{a}} \right) \\ \mu_k^L &= \beta_k \widetilde{r^*_{+k}} + \alpha_k r_{-k} = -\beta_k l_{+k} + \alpha_k r_{-k} \\ &= \frac{1}{\sqrt{4\pi\omega_k}\sqrt{2\sinh\frac{\pi\omega_k}{a}}} \left(e^{\frac{-\pi\omega_k}{2a}} \left(a(-t+x+i\epsilon)\right)^{\frac{-i\omega_k}{a}} + e^{\frac{\pi\omega_k}{2a}} \left(a(t+x-i\epsilon)\right)^{\frac{-i\omega_k}{a}} \right) \end{aligned} \tag{14}$$

Here, the tilde denotes opposite analytic continuation across the logarithmic branch cut, corresponding to the conjugate $i\epsilon$ prescription. Operationally, this captures the mode's behavior in the left wedge and is often written using left Rindler modes l_k and l_{-k}, which have opposite sign and live in coordinates related by $t \to -t$, $x \to -x$.

The functions μ_k^R and μ_k^L are analytic in the lower-half complex t-plane and decay at infinity, so they qualify as positive-frequency Minkowski modes. They form an alternative orthonormal basis of solutions to the Klein-Gordon equation, distinct from the plane waves $\varphi_{\pm k}$. The Unruh modes diagonalize the Minkowski vacuum in terms of Rindler particle states and thus provide the natural framework for describing the Unruh effect and the thermal response perceived by uniformly accelerated observers.

2.3 Bogoliubov Transforms

We generalize the wedge W to a translated wedge W_c with apex $(0, c)$

$$W_c = \{(t, x) : x - c > |t|\} \tag{15}$$

and a reflected (left) wedge $\widetilde{W}_c$ with apex $(0, c)$

$$\widetilde{W}_c = \{(t, x) : x - c < -|t|\}. \tag{16}$$

Let the superscripts (0), (c), $(\widetilde{c})$, and (M) represent the W_0, W_c, $\widetilde{W}_c$, and Minkowski frames of reference respectively. Let $(A \to B)$ represent an open set inclusion $A \subseteq B$ [4].

Since the analytically extended Rindler modes remain solutions of the Klein–Gordon equation, their inner products are preserved under continuation from the wedge to Minkowski space. This allows us to directly compute $W_0 \to M$ Bogoliubov coefficients from equation (14)

$$\left[\begin{array}{c} a_k^{(0)} \\ \hline a_{-k}^{(0)} \\ \hline a_k^{(0)\dagger} \\ \hline a_{-k}^{(0)\dagger} \end{array}\right] = \left[\begin{array}{cc|cc} \alpha_k & 0 & 0 & \beta_k \\ 0 & \alpha_k & \beta_k & 0 \\ \hline 0 & \beta_k & \alpha_k & 0 \\ \beta_k & 0 & 0 & \alpha_k \end{array}\right]_{k,q} \left[\begin{array}{c} c_q^R \\ \hline c_q^L \\ \hline c_q^{R\dagger} \\ \hline c_q^{L\dagger} \end{array}\right] \tag{17}$$

[4] In the Haag-Kastler framework[7] of algebraic quantum field theory, the assignment of von Neumann algebras to spacetime regions defines a covariant functor: the inclusion of regions $A \to B$ induces an inclusion of algebras $\mathcal{A}(A) \to \mathcal{A}(B)$. Conversely, the Bogoliubov transformation, when defined, given by $\alpha^{(A\to B)}$ and $\beta^{(A\to B)}$ defines a contravariant map in this paper.

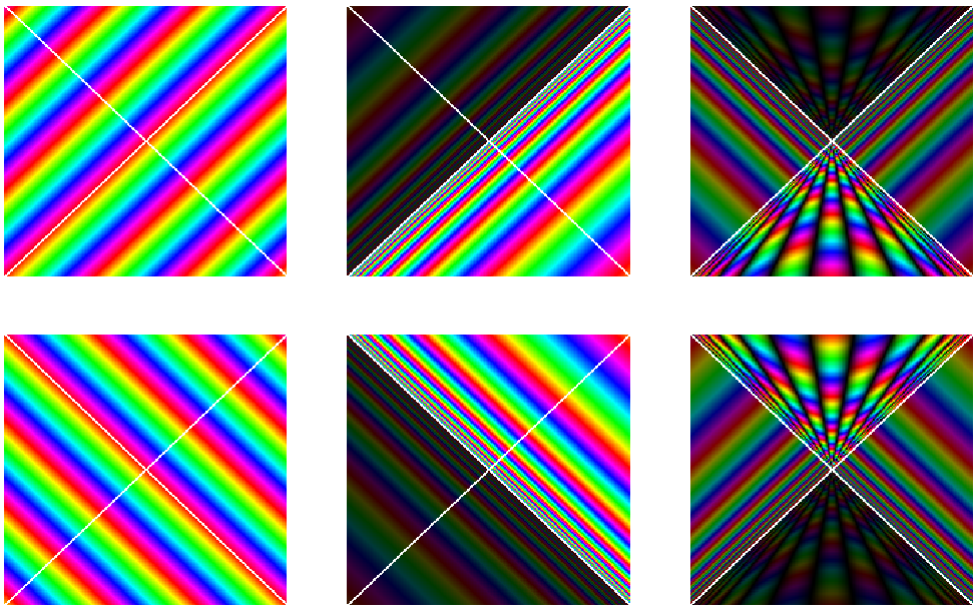

Figure 2: Spacetime diagrams of the $k > 0$ mode functions $\begin{bmatrix} \varphi_k & r_k & \mu_k^R \\ \varphi_{-k} & r_{-k} & \mu_k^L \end{bmatrix}$. Color encodes the phase; brightness indicates magnitude. The Minkowski modes φ_k and Unruh modes μ_k display consistent *rainbow* phase structure at $t = 0$, reflecting their global positive-frequency character. In contrast, the Rindler modes r_k flip phase across the horizon due to the analytic structure of the logarithm. The left-moving mode r_k corresponds to emission; the right-moving r_{-k} to absorption.

for a change of basis from $a_q^{(M)}$ to c_q^R and c_q^L

$$\phi = \int \mathrm{d}q \; \mu_q^R c_q^R + \mu_q^L c_q^L + \text{h.c.} \tag{18}$$

So that we can summarize the transform as

$$a_k^{(0)} = \alpha_k c_q^R + \beta_k c_q^{L\dagger} \tag{19}$$

We next compute the more general mixed Bogoliubov transformations.

$$\begin{aligned} (c \to M): \quad a_k^{(c)} &= \int \mathrm{d}q \; \alpha_{kq}^{(c\to M)} a_q^M + \beta_{kq}^{(c\to M)} a_q^{(M)\dagger} \\ (c \to 0): \quad a_k^{(c)} &= \int \mathrm{d}q \; \alpha_{kq}^{(c\to 0)} a_q^{(0)} + \beta_{kq}^{(c\to 0)} a_q^{(0)\dagger} \\ (\widetilde{c} \to 0): \quad a_k^{(\widetilde{c})} &= \int \mathrm{d}q \; \alpha_{kq}^{(\widetilde{c}\to 0)} a_q^{(0)} + \beta_{kq}^{(\widetilde{c}\to 0)} a_q^{(0)\dagger} \end{aligned} \tag{20}$$

We make use of a gamma function for $(c \to M)$. This occurs naturally in the KG dot product as an integral over an exponential phase from φ_k (the Mellin transform of e^{ikx} [8]) and a $(x - c)$ power from $r_k^{(c)}$:

$$\begin{aligned} \alpha_{kq}^{(c\to M)} &= \left\langle \varphi_q, r_k^{(c)} \right\rangle = \tfrac{1}{a\pi} \sqrt{\tfrac{\omega_k}{\omega_q}} \left(\tfrac{a}{q}\right)^{\frac{i\omega_k}{a}} e^{\frac{\pi\omega_k}{a}} \Gamma\left(\tfrac{i\omega_k}{a}\right) \\ \beta_{kq}^{(c\to M)} &= \left\langle \varphi_q^*, r_k^{(c)} \right\rangle = \tfrac{1}{a\pi} \sqrt{\tfrac{\omega_k}{\omega_q}} \left(\tfrac{a}{q}\right)^{\frac{-i\omega_k}{a}} e^{\frac{-\pi\omega_k}{a}} \Gamma\left(\tfrac{-i\omega_k}{a}\right) \end{aligned} \tag{21}$$

Next we consider products of shifted powers to go after $(c \to 0)$. We make use of a beta function for $(c \to 0)$ which occurs naturally in the KG dot product as an integral over

a power of x and of $x-c$, from $r_k^{(0)}$ and $r_k^{(c)}$ respectively. We compute the Bogoliubov coefficients as

$$\begin{aligned}\alpha_{kq}^{(c\to 0)} &= \left\langle r_q^{(0)}, r_k^{(c)} \right\rangle = \frac{1}{2\pi a}\sqrt{\frac{\omega_k}{\omega_q}}(ac)^{\frac{i(\omega_k-\omega_q)}{a}} B\left(\frac{i\omega_k}{a}, \frac{-i(\omega_k-\omega_q)}{a}\right) \\ \beta_{kq}^{(c\to 0)} &= \left\langle r_q^{(0)*}, r_k^{(c)} \right\rangle = \frac{1}{2\pi a}\sqrt{\frac{\omega_k}{\omega_q}}(ac)^{\frac{i(\omega_k+\omega_q)}{a}} B\left(\frac{i\omega_k}{a}, \frac{-i(\omega_k+\omega_q)}{a}\right)\end{aligned} \tag{22}$$

The reflected diamond wedge version also yields a beta function, but with a different form

$$\begin{aligned}\alpha_{kq}^{(\widetilde{c}\to 0)} &= \left\langle r_q^{(0)*}, r_k^{(\widetilde{c})} \right\rangle = \frac{1}{2\pi a}\frac{\sqrt{\omega_k\omega_q}}{\omega_q-\omega_k}(ac)^{\frac{i(\omega_k-\omega_q)}{a}} B\left(\frac{i\omega_k}{a}, -\frac{i\omega_q}{a}\right) \\ \beta_{kq}^{(\widetilde{c}\to 0)} &= \left\langle r_q^{(0)}, r_k^{(\widetilde{c})} \right\rangle = \frac{1}{2\pi a}\frac{\sqrt{\omega_k\omega_q}}{\omega_q+\omega_k}(ac)^{\frac{i(\omega_k+\omega_q)}{a}} B\left(\frac{i\omega_k}{a}, \frac{i\omega_q}{a}\right)\end{aligned} \tag{23}$$

We can compare absolute magnitudes for M v.s. W_c and see that they don't depend on q or c

$$\begin{aligned}\left|\beta_{kq}^{(c_1\to M)}\right|^2 &= \left|\beta_{kq}^{(c_2\to M)}\right|^2 \\ \left|\beta_{kq}^{(c_1\to M)}\right|^2 &= \left|\beta_{kq}^{(c_2\to M)}\right|^2\end{aligned} \tag{24}$$

The c independence is expected since Unruh radiation is translation invariant. The q independence can be strengthened as the expected number of particles in mode k

$$\int \mathrm{d}q \ \left|\beta_{kq}^{(c\to M)}\right|^2 = \frac{e^{\frac{-2\pi\omega_k}{a}}}{2\sinh\frac{\pi\omega_k}{a}}\int \mathrm{d}q \ \frac{2}{a\pi|q|} \tag{25}$$

where we factor out the divergent part to recover the radiation equation again[5].

We next turn to $(c\to 0)$ and also find c independence there

$$\begin{aligned}\left|\alpha_{kq}^{(c_1\to 0)}\right| &= \left|\alpha_{kq}^{(c_2\to 0)}\right| \\ \left|\beta_{kq}^{(c_1\to 0)}\right| &= \left|\beta_{kq}^{(c_2\to 0)}\right|\end{aligned} \tag{26}$$

which is somewhat more surprising since this implies that $\int \mathrm{d}q \ \left|\beta_{kq}^{(c_2\to c_1)}\right|^2$ are c_1 and c_2 independent quantities for every shifted (and reflected resp.) wedge inclusion.

In other words, for shifted wedges[6], the expected number of particles for a mode $r_k^{(c_2)}$ of W_{c_2} in W_{c_1}'s vacuum is independent of the choice of shift c_2 and c_1. More explicitly we have a transform matrix of Λ_c from W_0 to W_c

$$\begin{bmatrix} a_k^{(c)} \\ a_{-k}^{(c)} \\ \hline a_k^{(c)\dagger} \\ a_{-k}^{(c)\dagger} \end{bmatrix} = \underbrace{\left[\begin{array}{cc|cc} A_c & 0 & B_c & 0 \\ 0 & -A_c & 0 & -B_c \\ \hline \overline{B_c} & 0 & \overline{A_c} & 0 \\ 0 & -\overline{B_c} & 0 & -\overline{A_c} \end{array}\right]_{k,q}}_{\Lambda_c} \begin{bmatrix} a_q^{(0)} \\ a_{-q}^{(0)} \\ \hline a_q^{(0)\dagger} \\ a_{-q}^{(0)\dagger} \end{bmatrix} \tag{27}$$

where $A_c = \alpha_{kq}^{(c\to 0)} = P_c A_1 P_c^{-1}$ and $B_c = \beta_{kq}^{(c\to 0)} = P_c B_1 P_c$ for a diagonal phase factor matrix

$$P_c = P_{c,rs} = \delta(r-s)c^{\frac{i\omega_r}{a}} = e^{\frac{iH}{a}\log c} \tag{28}$$

We can write Λ_c out compactly out as

$$\Lambda_c = Q_c \Lambda_1 Q_c^{-1} \tag{29}$$

[5]We frequently use here and elsewhere $|\Gamma(ib)|^2 = \frac{\pi}{b\sinh\pi b}$

[6]Similar statements are true for reflected (diamond) wedge inclusions

where

$$Q_c = \begin{bmatrix} P_c, & 0 & 0 & 0 \\ 0 & P_c & 0 & 0 \\ 0 & 0 & P_c^{-1} & 0 \\ 0 & 0 & 0 & P_c^{-1} \end{bmatrix} \tag{30}$$

Note that $\lim_{c\to 0} \Lambda_c = 1$ since the limit of $\lim_{c\to 0} \alpha_{kq}^{(c\to 0)} = 1$ and $\lim_{c\to 0} \beta_{kq}^{(c\to 0)} = 0$, which corresponds nicely to $\lim_{c\to 0} W_c = W_0$. The composition of Bogoliubov transforms, $\Lambda_{nc} = \Lambda_c^n$, yields

$$\begin{aligned} Q_{nc}\Lambda_1 Q_{nc}^{-1} &= \Lambda_{nc} \\ &= (Q_c\Lambda_c Q_c)\left(Q_c^{-1}\Lambda_c Q_c\right)\cdots(Q_c\Lambda_c Q_c) \\ &= Q_c\Lambda_c^n Q_c^{-1} \end{aligned} \tag{31}$$

so that

$$\begin{aligned} \Lambda_c^n &= Q_c^{-1}Q_{nc}\Lambda_1 Q_{nc}^{-1}Qc \\ &= Q_n\Lambda_1 Q_n^{-1} \end{aligned} \tag{32}$$

and more generally we have a one parameter group given by

$$\left\{\Lambda_0^x = Q_x\Lambda_0 Q_x^{-1} : x \in \mathbb{R}\right\}. \tag{33}$$

These Bogoliubov transformations between shifted wedges define a one-parameter group, reflecting an underlying symmetry structure. This naturally connects to modular flow as studied in algebraic QFT, where such transformations correspond to automorphisms generated by the modular operator. This is an explicit realization of modular flow, due to the von Neumann algebra modular automorphism associated with the translation $W_0 \to W_c$, studied in detail in Tomita-Takesaki theory [9]. There we find thermal KMS states between open set inclusions in a much more general setting. A key distinction from the standard approach is that, rather than focusing on Lorentz boosts within a fixed wedge, we examine modular structures associated with spacetime translations and reflections across different wedges.

Consider a sequence

$$W_{c_n} \subseteq \cdots \subseteq W_{c_i} \subseteq \cdots \subseteq W_{c_j} \subseteq W_{c_2} \subseteq W_{c_1} \tag{34}$$

Then each $W_{c_i} \subseteq W_{c_j}$ involves particle production with a fixed squared magnitude for mode k. We calculate this expected number of W_{c_i} particles for mode k in W_{c_j}'s vacuum

$$\langle 0_{W_{c_j}} | \, a_k^{(c_i)\dagger} a_k^{(c_i)} \, |0_{W_{c_j}}\rangle = \frac{1}{2\pi^2 k \sinh\frac{\pi k}{a}} \int_{x=0}^{\infty} \frac{x\sinh x}{(x+\frac{\pi k}{a})\sinh(x+\frac{\pi k}{a})} \tag{35}$$

which diverges. The integrand goes to $e^{-\frac{\pi k}{a}}$ as x gets large, so we can see that the expected number of particles in ratio goes to another thermal form

$$\frac{1}{m(e^{2m}+1)} = \frac{1}{k(e^{\frac{2\pi\omega_k}{a}}-1)}. \tag{36}$$

3 Driving Sources

We now turn to a foundational question: **"What, physically, is accelerating the observer?"** Up to this point, acceleration has been introduced as a geometric feature, a coordinate choice, without reference to any underlying dynamical mechanism. Moreover, we have left unspecified both the observer's precise location within the Rindler wedge and the spatial origin of the detected excitations. These omissions reflect an effective coarse-graining over the details of the observer and their interaction with the field, a feature that contributes to the apparent thermality observed in the Unruh effect.

Figure 3 illustrates the structure of a sharply peaked frequency wave packet composed of Rindler modes. The modes r_k are left-moving, propagating toward the future horizon and interpreted as **emission**; the r_{-k} modes are right-moving, originating from the past horizon and interpreted as **absorption**. These Rindler modes are constructed as superpositions of Minkowski modes φ_q, effectively smeared across a range of frequencies. This frequency mixing is evident in Figure 2, where the local frequencies shift, blue-shifting near the horizons due to the geometry of the wedge.

The mathematical underpinning of this effect is encoded in the Bogoliubov coefficients $\alpha_{kq}^{(c\to M)}$ and $\beta_{kq}^{(c\to M)}$, which express the Rindler modes in terms of their Klein-Gordon inner products with Minkowski positive- and negative-frequency modes, φ_q and φ_q^*, respectively. This delocalization in frequency space, rooted in the extended support of the Rindler modes and tied to the observer's causal horizon, plays a central role in producing the thermal spectrum characteristic of the Unruh effect.

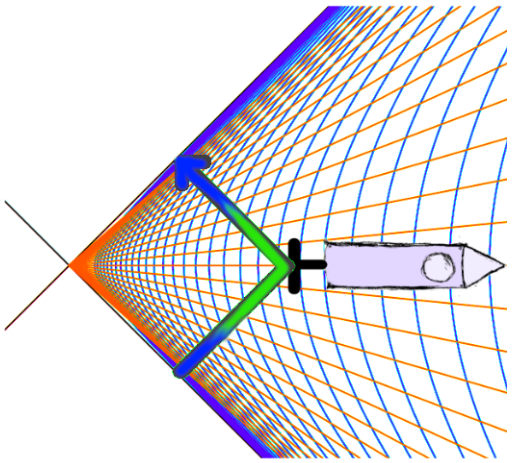

Figure 3: A Rindler mode's frequency is smeared out in Minkowski space, blue-shifted near the horizon. We diagram a particle as if it were striking a mirror at the rear of a rocket, where its reflection emerges as a combination of emission and absorption processes in the Rindler frame.

To address this, we introduce a driving source [3] [10], a physical mechanism that excites the field and, indirectly, accounts for the observer's acceleration. This reframes the interpretation: the observed radiation is not spontaneous, but emerges as a coherent, dynamical response to an external influence. An illustration of this setup is shown in Figure 4. From this perspective, the apparent thermality arises not from intrinsic properties of the vacuum, but from an effective ignorance of the source's detailed structure and dynamics.

To model this process, we aim to match the effect of a field-theoretic creation operator by introducing a classical source term $J(x)$ into the Lagrangian, applied at an early time. The source couples linearly to the field and excites a specific mode, thereby preparing a coherent state whose phase and amplitude are determined by the source profile. In order to replicate the targeted excitation, $J(x)$ must be engineered so that its inner product with the mode functions $u_k(x)$ matches the effect of the creation operator acting on the vacuum.

The field can be expanded as in equation (18), and the β_k-term in equation (19) is responsible for the thermal particle content of the Minkowski vacuum as seen by Rindler observers. For clarity, we first present the construction for a single positive-frequency μ_k^{L*}-mode. Because the Unruh modes form a complete orthonormal set under the Klein-Gordon inner product, this construction extends linearly and independently to the full

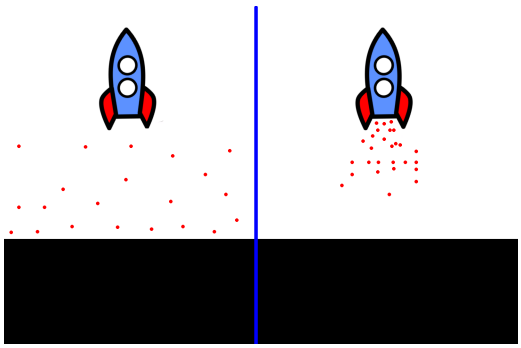

Figure 4: Conceptual illustration of thermal v.s. localized acceleration.

family of modes. We encode the effect of a creation operator $c_k^{L\dagger}$ using

$$c_k^{L\dagger} = \left\langle \phi, \mu_k^{L*} \right\rangle_{KG} = \int \mathrm{d}x \; \mu_k^{L*}(x)\phi(x) \tag{37}$$

and the orthogonality of the mode functions in the Klein-Gordon inner product.

Although the Unruh modes involve both left- and right-moving Rindler components, associated with emission and absorption in the accelerated frame, they are constructed to have purely negative frequency with respect to Minkowski time. This ensures that the source couples to physical creation operators and injects particles into the field in a well-defined way. The resulting excitation respects the correct Minkowski vacuum structure while encoding the full Rindler response.

In the generating functional formalism, setting $J_k^L(x) = -\beta_k u_k^{L*}$ the functional derivative $\frac{\delta}{\delta J_k^L} Z[J_k^L]|_{J_k^L=0}$ inserts ϕ into time-ordered correlators. Smearing this field insertion against $\mu_k^{L*}(x)$ thus projects onto $c_k^{L\dagger}$ and we have[7]

$$\begin{aligned} a_k^{(0)J} &= \alpha_k c_q^R + \beta_k c_q^{L\dagger} - \beta_k c_q^{L\dagger} \\ &= \alpha_k c_q^R \end{aligned} \tag{38}$$

In Rindler coordinates, the presence of this source term prepares a modified field state in which the Rindler mode occupation deviates from the thermal distribution that characterizes the Minkowski vacuum. Rather than simply injecting energy into the field, the source introduces a coherent excitation that interferes with the mode structure induced by the Bogoliubov β-terms. In effect, the source replaces the contribution of these terms for the selected mode, allowing us to construct a state in which the Rindler detector response becomes vacuum-like for a given mode k:

$$\langle J_k^L |\, b_k^\dagger b_k \,| J_k^L \rangle = \langle 0_M |\, b_k^{J_k^L\dagger} b_k^{J_k^L} \,| 0_M \rangle = 0 \tag{39}$$

This construction reproduces the Rindler particle spectrum predicted by the Bogoliubov transformation, but with a key difference: the observed response now results from a well-defined dynamical process rather than a statistical average over inaccessible degrees of freedom. Provided the excited modes form a Klein-Gordon orthonormal basis—such as the Unruh modes—this equivalence holds when using causal (retarded) or time-ordered (Feynman) Green's functions. These propagators allow linear superpositions of negative-frequency components to act as physically realizable particle injections.

[7]The remaining α_k factor reflects the mismatch between the squeezed Unruh vacuum and the coherent state prepared by the source.

4 Sub-wedge Localization in Rindler Space

4.1 Localization via Translated Wedge Inclusion

Consider the two nested Rindler wedges $W_c \subseteq W_0$ shown in Figure 5. Let r_q denote a Rindler mode associated with W_0, analytically continued to the entire Minkowski space. The gray-scale region indicates the full support of r_q, while the rainbow-colored segment shows its restriction to the smaller wedge W_c.

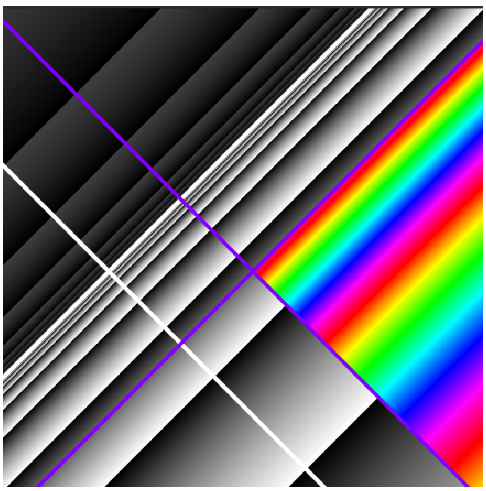

Figure 5: A Wedge W_c (blue) inside of the wedge W_0 (white). Rindler mode r_q of W_0 (gray-scale) restricted to W_c (rainbow).

By considering the restriction of r_q to W_c, we have partially localized the observer and the mode. The restriction effectively cuts off the high-frequency content of r_q near the future horizon[8]. The resulting mode still spans the full spatial extent of W_c, but it is now insulated from the highly oscillatory behavior near the horizons of W_0. The localization is not complete however, the observer can still be anywhere within the wedge W_c, and the corresponding modes r_k still exhibit thermal characteristics because of low-frequency oscillations extending throughout the wedge.

To further study the situation, consider the modulus squared inner product $\left|\left\langle r_q^{(0)}, r_k^{(c)} \right\rangle\right|^2$, also known as the Bogoliubov $\left|\alpha_{kq}^{(c\to 0)}\right|^2$, from equation (22). We fix q and view

$$\left|\left\langle r_q^{(0)}, r_k^{(c)} \right\rangle\right|^2 = \frac{\sinh \frac{\pi\omega_q}{a}}{4\pi a(\omega_q - \omega_k) \sinh \frac{\omega_q - \omega_k}{a} \sinh \frac{\pi\omega_k}{a}} \tag{40}$$

as a function of ω_k. The function exhibits a second-order pole at $\omega_k = \omega_q$, resulting in a sharply peaked spectral response, see Figure 6. The thermal character is evident in the sinh terms: $\sinh \frac{\pi\omega_k}{a}$ introduces a broadening near $\omega_k = 0$, while $\sinh \frac{\omega_q - \omega_k}{a}$ contributes thermal spreading near the peak at $\omega_k = \omega_q$. However, the pronounced spectral peak at $\omega_k = \omega_q$ arises not from thermal effects but from the localization itself.

4.2 Diamond Localization via Reflected Wedge Intersection

Further localization is achieved by intersecting W_c with a reflected wedge $\widetilde{W}_{2c}$. This defines a more tightly localized diamond-shaped region, as shown in Figure 7. The mode r_q is now restricted to the intersection $W_c \cap \widetilde{W}_{2c}$, which eliminates much of the infrared divergence previously associated with the unrestricted wedge.

[8]Similarly, r_{-q} experiences suppression near the past horizon.

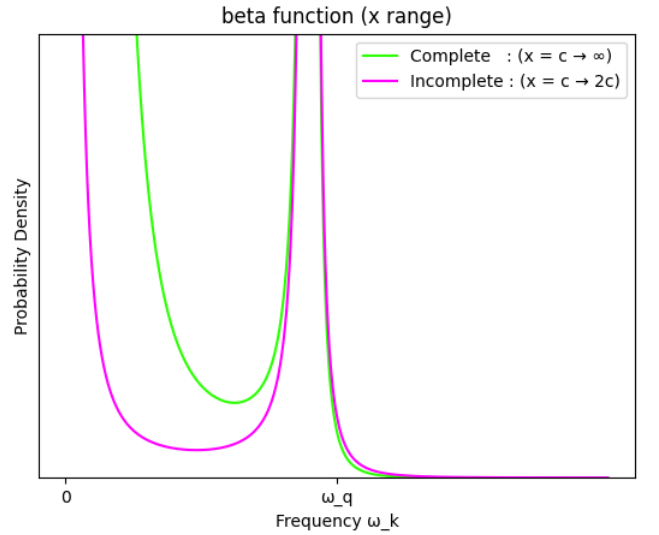

Figure 6: The Rindler modes r_k of W_c show a peaked spectral overlap with r_q at $\omega_k = \omega_q$. The incomplete beta function picks out the spectral peak suppressing the peak at zero.

The Klein Gordon inner product at $t = 0$ now takes the form of an incomplete version of the beta function from equation (22), corresponding to an integral[9] evaluated from c to $2c$ rather than extending to infinity. This inner product does not however correspond to a mode expansion of the field, since the analytic continuation of the diamond would be to all of W_c, or all of $\widetilde{W}_{2c}$, in which case we would no longer be localized to the diamond. So it is no longer invariant to integrate along a Cauchy surface for the inner product; this construction does not define a complete orthonormal set, and cannot be used to build a full basis of field modes.

Instead, we can take the viewpoint that the diamond is a localized driving source, as in Section 3; we are no longer interpreting r_q as a solution to the free Klein-Gordon equation everywhere, but as a compact test function that drives a response in the field. We turn on r_q exactly for a fixed period of $x - t$ (or $x + t$ for r_{-q}). The resulting spectral response in the diamond, computed from this truncated integral, is shown in Figure 6. The plot reveals that the main spectral peak at $\omega_k = \omega_q$ persists, while the thermal contribution near $\omega = 0$ is significantly attenuated.

4.3 Thermal to Localized Mode Interpolation

We will next explore a method to interpolate between thermal and localized modes. We use parabolic cylinder functions [11, 13] which are the analytic continuation of

$$D_\nu(-z) = \frac{e^{-\frac{1}{4}z^2}}{\Gamma(-\nu)} \int_0^\infty e^{zs} s^{-\nu-1} e^{-\frac{1}{2}s^2} \mathrm{d}s \ , \Re\nu < 0, \tag{41}$$

where we use $-z$ instead of the usual z so that future equations become simpler.

Without loss of generality, let $N_{\mu,\sigma} = e^{-\frac{1}{2}\frac{(x-t-\mu)^2}{\sigma^2}}$ be a (left-moving) Gaussian kernel with fixed μ. We will multiply φ_q^* by $N_{\mu,\sigma}$ but we could just as easily multiply r_k by $N_{\mu,\sigma}$ for the same effect. A key aspect of this construction is that the resulting Minkowski modes are treated as driving sources rather than elements of an orthonormal mode expansion. Since we are not working within an orthonormal mode expansion, the normalization of

[9] We could also use the beta function in equation (23) to compute the same inner product using the alternative incomplete beta function.

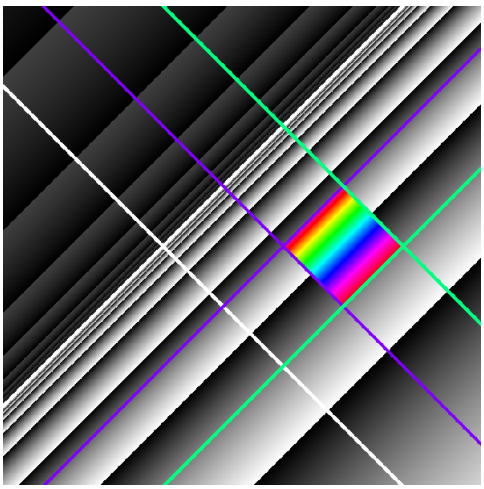

Figure 7: The same situation as in Figure 5 but we further intersect with a reflected (left) wedge $\widetilde{W}_{2c}$ (green). Rindler mode r_q of W_0 (gray-scale) restricted to $W_c \cap \widetilde{W}_{2c}$ (rainbow).

$N_{\mu,\sigma}$ is left implicit, though relative magnitudes may be compared later. For clarity, since this setup may be non-standard, we carry out the calculations explicitly in this section. We will examine the $N_{\mu,\sigma}$ modification of $\beta_{kq}^{(c\to M)}$ in equation (21)

$$\begin{aligned}
\left\langle \varphi_q^* N_{\mu,\sigma}, r_k \right\rangle &= \frac{1}{4\pi\sqrt{\omega_q\omega_k}} 2i \int_{\Sigma_W} e^{-i(\omega_q t - qx)} e^{-\frac{1}{2}\frac{(x-t-\mu)^2}{\sigma^2}} \partial_t (a(x-t))^{\frac{i\omega_k}{a}} \\
&= \frac{1}{2\pi}\sqrt{\frac{\omega_k}{\omega_q}} a^{\frac{i\omega_k}{a}-1} \int_0^\infty e^{-\frac{1}{2}\frac{(x-\mu)^2}{\sigma^2}+iqx} x^{\frac{i\omega_k}{a}-1} \mathrm{d}x \\
&= \frac{1}{2\pi}\sqrt{\frac{\omega_k}{\omega_q}} a^{\frac{i\omega_k}{a}-1} \int_0^\infty e^{\left(-\frac{1}{2\sigma^2}\right)x^2+\left(\frac{\mu}{\sigma^2}+iq\right)x+\left(-\frac{\mu^2}{2\sigma^2}\right)} x^{\frac{i\omega_k}{a}-1} \mathrm{d}x \\
&= \frac{1}{2\pi a}\sqrt{\frac{\omega_k}{\omega_q}} e^{-\frac{\mu^2}{2\sigma^2}} \sigma^{\frac{i\omega_k}{a}} a^{\frac{i\omega_k}{a}} \int_0^\infty e^{(\frac{\mu}{\sigma}+iq\sigma)s} s^{\frac{i\omega_k}{a}-1} e^{-\frac{1}{2}s^2} \mathrm{d}s \\
&= \frac{1}{2\pi a}\sqrt{\frac{\omega_k}{\omega_q}} e^{-\frac{\mu^2}{2\sigma^2}} (\sigma a)^{\frac{i\omega_k}{a}} e^{\frac{1}{4}(iq\sigma+\frac{\mu}{\sigma})^2} \Gamma\left(\frac{i\omega_k}{a}\right) D_{-\frac{i\omega_k}{a}}(-iq\sigma - \frac{\mu}{\sigma}) \\
&= \frac{1}{2\pi a}\sqrt{\frac{\omega_k}{\omega_q}} e^{-\frac{\mu^2}{2\sigma^2}} (\sigma a)^{\frac{i\omega_k}{a}} e^{\frac{1}{4}z^2} \Gamma(-\nu) D_\nu(-z)
\end{aligned} \tag{42}$$

where Σ_W is the Cauchy surface $\eta = 0$ on the Rindler wedge W, $x = \sigma s$, $z = iq\sigma + \frac{\mu}{\sigma}$, and $\nu = -\frac{i\omega_k}{a}$. And then

$$\left|\left\langle \varphi_q^* N_{\mu,\sigma}, r_k \right\rangle\right|^2 = \frac{1}{2\pi a\omega_q} \frac{\omega_k}{2\pi a} e^{-\frac{\mu^2}{\sigma^2}} \left| e^{\frac{1}{2}z^2} \right| |\Gamma(-\nu)|^2 \, |D_\nu(-z)|^2 \tag{43}$$

From [13] we have

$$D_\nu(-z) = e^{-i\pi\nu} z^\nu e^{-\frac{1}{4}z^2} \{1 + O(|z|^{-2})\} + \frac{(2\pi)^{\frac{1}{2}}}{\Gamma(-\nu)} z^{-\nu-1} e^{\frac{1}{4}z^2} \{1 + O(|z|^{-2})\} \tag{44}$$

when $-\frac{1}{4}\pi + \epsilon \le \arg z \le \frac{3}{4}\pi - \epsilon$. The second $e^{\frac{1}{4}z^2}$ term dominates for $z \to \infty$ as $\sigma \to 0$ and the first $e^{-\frac{1}{4}z^2}$ term dominates for $z \to i\infty$ as $\sigma \to \infty$. This is a Stokes phenomenon[10]

[10]See [12] for a similar approach where the Stokes phenomenon is applied to particle production in simple expanding backgrounds, preheating after R^2 inflation, and a transition model with smoothly changing mass.

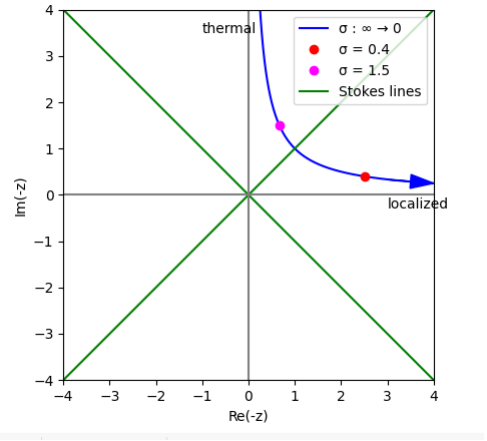

Figure 8: Stokes phenomenon for the parabolic cylinder function as σ interpolates between ∞ and 0. The Stokes curve is passed at $\arg z = \frac{\pi}{4}$. Some values for σ are marked, see also corresponding Figure 9.

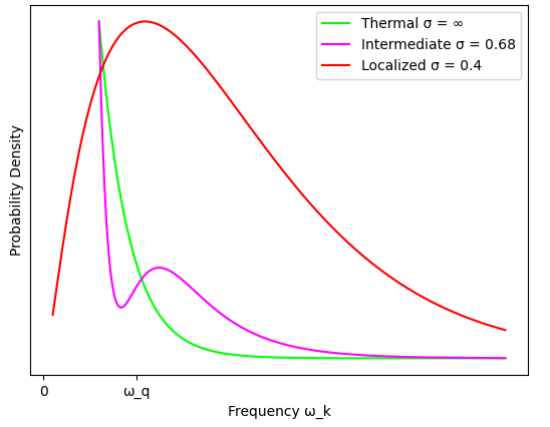

Figure 9: $\left|\left\langle \varphi_q^* N, r_k \right\rangle\right|^2$ for various values of σ (probability density is scaled for comparision). $\omega_q = 1$, $q = 1$, $a = 1$, $\mu = 1$. See also corresponding Figure 8.

which flips over as we cross the Stokes line at $\arg z = \frac{\pi}{4}$. The situation is pictured in Figure 8.

We next combine equations (43) and (44). First for the thermal part that comes from the $e^{-\frac{1}{4}z^2}$ term where $\sigma \to \infty$ we have

$$\begin{aligned}
2\pi a \omega_q \left|\left\langle \varphi_q^* N, r_k \right\rangle\right|^2 &= \frac{\omega_k}{2\pi a} e^{-\frac{\mu^2}{\sigma^2}} \left| e^{-i\pi\nu} z^\nu \Gamma\left(\frac{i\omega_k}{a}\right)\right|^2 \\
&= \frac{\omega_k}{2\pi a} e^{-\frac{\mu^2}{\sigma^2}} e^{\frac{-2\pi\omega_k}{a}} \left| e^{\frac{-2i\omega_k}{a}\log\left(\frac{\mu}{\sigma}+iq\sigma\right)}\right|^2 \frac{\pi}{\frac{\omega_k}{a}\sinh\frac{\pi\omega_k}{a}} \\
&\to e^{\frac{-2\pi\omega_k}{a}} \left| e^{\frac{-2i\omega_k}{a}\log i}\right|^2 \frac{1}{2\sinh\frac{\pi\omega_k}{a}} \\
&= e^{\frac{-2\pi\omega_k}{a}} e^{\frac{\pi\omega_k}{a}} \frac{1}{\left(e^{\frac{\pi\omega_k}{a}} - e^{\frac{-\pi\omega_k}{a}}\right)} \\
&= \frac{1}{e^{\frac{2\pi\omega_k}{a}} - 1}
\end{aligned} \tag{45}$$

which we expect by construction. For the localized part that comes from the $e^{\frac{1}{4}z^2}$ term where $\sigma \to 0$ we have

$$\begin{aligned} 2\pi a\omega_q \left|\left\langle \varphi_q^* N, r_k \right\rangle\right|^2 &= \frac{\omega_k}{a} e^{-\frac{\mu^2}{\sigma^2}} \left| e^{z^2} z^{2(-\nu-1)} \right| \\ &= \frac{\omega_k}{a} e^{-\frac{\mu^2}{\sigma^2}} \left| e^{\left(iq\sigma+\frac{\mu}{\sigma}\right)^2} e^{2\left(\frac{i\omega_k}{a}-1\right)\log\left(iq\sigma+\frac{\mu}{\sigma}\right)} \right| \\ &\to \frac{\omega_k}{a}\frac{\sigma^2}{\mu^2} \end{aligned} \tag{46}$$

where the thermal pole at zero has disappeared. We should stop short of σ actually reaching zero, since that is a localization to an extreme, where $N_{\mu,\sigma}$ shrinks to a bump with infinitesimal width; This is not a delta function, it is a vanishing source. We should not worry too much about the final form[11], but once we pass the Stokes line we find ourselves in a localized setting for small nonzero σ. For an example, see Figure 9 for a plot for various values of σ.

5 Conclusion

This work explored the Unruh phenomenon from a localized perspective, emphasizing its manifestation as a physically driven effect rather than a purely thermal one. By restricting Rindler modes to translated, reflected wedges, and their intersections, we demonstrated that the apparent thermal behavior could be partially eliminated as we localized the Rindler modes to get a spectrally peaked response in the Rindler sub-wedges. We then showed that the mixed Bogoliubov inner product between Minkowski and Rindler modes admits a smooth interpolation from global thermality to a localized spectral structure, with parabolic cylinder functions encoding this transition in analytic form.

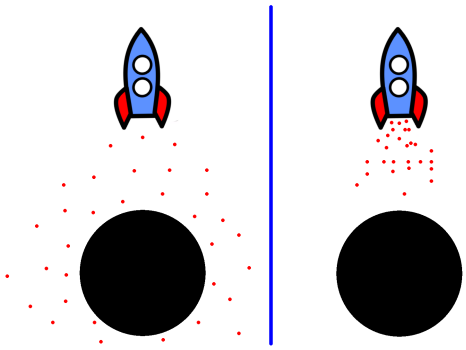

Figure 10: Conceptual illustration of thermal Hawking radiation v.s. local acceleration.

While our analysis is grounded in flat spacetime, the equivalence principle offers a natural pathway for extending this framework to curved spacetimes. In particular, future work could apply this approach to the context of Hawking radiation by modeling localized excitations near black hole horizons. This is illustrated schematically in Figure 10, which depicts a representative localized response in the near-horizon region.

[11] Instead of letting z go to ∞ we can let it go to $(1+i\epsilon)\infty$ which is still in the localized Stokes region. Then we end up multiplying the $\frac{\omega_k}{a}$ by a term like $e^{\frac{-2\epsilon\omega_k}{a}}$ to control the final form in the ultraviolet. This doesn't really matter though since we are more concerned with a small but nonzero σ where the thermal character has disappeared.

6 Acknowledgments

Thanks to Ben Commeau, Daniel Justice, and Edward Randtke for useful discussions.

References

[1] W. G. Unruh, "Notes on black-hole evaporation," *Physical Review D*, vol. 14, no. 4, p. 870, 1976.

[2] L. C. Crispino, A. Higuchi, and G. E. Matsas, "The unruh effect and its applications," *Reviews of Modern Physics*, vol. 80, no. 3, pp. 787–838, 2008.

[3] J. Schwinger, "Particles and sources," *Physical Review*, vol. 152, p. 1219â€"1226, Dec. 1966.

[4] E. Frodden and N. Valdes, "Unruh effect: Introductory notes to quantum effects for accelerated observers," *International Journal of Modern Physics A*, vol. 33, no. 27, p. 1830026, 2018.

[5] T. Jacobson, "Introduction to quantum fields in curved spacetime and the hawking effect," in *Lectures on quantum gravity*, pp. 39–89, Springer, 2005.

[6] W. Rindler, "Kruskal space and the uniformly accelerated frame," *Am. J. Phys*, vol. 34, no. 12, pp. 1174–1178, 1966.

[7] R. Haag and D. Kastler, "An algebraic approach to quantum field theory," *Journal of Mathematical Physics*, vol. 5, no. 7, pp. 848–861, 1964.

[8] R. Bracewell and P. B. Kahn, "The fourier transform and its applications," *American Journal of Physics*, vol. 34, no. 8, pp. 712–712, 1966.

[9] H. J. Borchers, "On revolutionizing quantum field theory with tomita's modular theory," *Journal of mathematical Physics*, vol. 41, no. 6, pp. 3604–3673, 2000.

[10] L. H. Ryder, *Quantum field theory*. Cambridge university press, 1996.

[11] M. Abramowitz and I. A. Stegun, eds., *Handbook of Mathematical Functions with Formulas, Graphs, and Mathematical Tables*, vol. 55 of *Applied Mathematics Series*. Washington, D.C.: U.S. Government Printing Office, 1964. Reprinted 1983. See Chapter 19.

[12] S. Hashiba and Y. Yamada, "Stokes phenomenon and gravitational particle production—how to evaluate it in practice," *Journal of Cosmology and Astroparticle Physics*, vol. 2021, no. 05, p. 022, 2021.

[13] F. W. J. Olver, "Uniform asymptotic expansions for weber parabolic cylinder functions of large orders," *Journal of Research of the National Bureau of Standards. Section B, Mathematical Sciences*, vol. 63B, pp. 131–169, 1959.